

Measurements of Ca II absorption, metals, and dust in a sample of $z \simeq 1$ DLAs and subDLAs*

Daniel B. Nestor¹, Max Pettini¹, Paul C. Hewett¹, Sandhya Rao², and Vivienne Wild³

¹*Institute of Astronomy, University of Cambridge, Madingley Road, Cambridge CB3 0HA, UK*

²*Department of Physics and Astronomy, University of Pittsburgh, Pittsburgh, PA 15260, USA*

³*Max-Planck-Institut für Astrophysik, 85748 Garching, Germany*

Accepted —; Received —; in original form —

ABSTRACT

We present observations of Ca II, Zn II and Cr II absorption lines in 16 damped Lyman alpha systems (DLA) and six subDLAs at redshifts $0.6 < z_{\text{abs}} < 1.3$, obtained for the dual purposes of: (i) clarifying the relationship between DLAs and absorption systems selected from their strong Ca II lines, and (ii) increasing the still limited sample of Zn and Cr abundance determinations in this redshift range. We find only partial overlap between current samples of intermediate redshift DLAs (which are drawn from magnitude limited surveys) and strong Ca II absorbers: approximately 25 per cent of known DLAs at these redshifts have an associated Ca II $\lambda 3935$ line with a rest-frame equivalent width greater than 0.35 \AA , the threshold of the Sloan Digital Sky Survey sample assembled by Wild and her collaborators. The lack of the strongest Ca II systems (with equivalent widths greater than 0.5 \AA) is consistent with these authors' conclusion that such absorbers are often missed in current DLA surveys because they redden and dim the light of the background QSOs.

We rule out the suggestion that strong Ca II absorption is associated exclusively with the highest column density DLAs. Furthermore, we find no correlation between the strength of the Ca II lines and either the metallicity or degree of depletion of refractory elements, although the strongest Ca II absorber in our sample is also the most metal-rich DLA yet discovered, with $[\text{Zn}/\text{H}] \simeq$ solar. We conclude that a complex mix of parameters must determine the strengths of the Ca II lines, including the density of particles and ultraviolet photons in the interstellar media of the galaxies hosting the DLAs. We find tentative evidence (given the small size of our sample) that strong Ca II systems may preferentially sample regions of high gas density, perhaps akin to the DLAs exhibiting molecular hydrogen absorption at redshifts $z > 2$. If this connection is confirmed, strong Ca II absorbers would trace possibly metal-rich, H_2 -bearing columns of cool, dense gas at distances up to tens of kpc from normal galaxies.

Key words: Quasars: absorption lines – galaxies: abundances – galaxies: ISM – galaxies: haloes – intergalactic medium

1 INTRODUCTION

Quasar absorption lines are a powerful tool for the study of gaseous galactic structures over cosmic time, providing clues to the nature and evolution of galaxies and galactic halos. The large columns of neutral hydrogen gas traced by damped Lyman alpha (DLA) and subDLA systems (con-

ventionally defined to have H I column densities $N(\text{H I}) \geq 10^{20.3}$ atoms cm^{-2} and $10^{19} \leq N(\text{H I}) < 10^{20.3}$ atoms cm^{-2} respectively) are of particular interest (Rao 2005; Wolfe, Gawiser, & Prochaska 2005), as they account for most of the neutral gas in the Universe and trace galaxies which are often difficult to detect directly. Thus, appropriate to their importance, much effort has been expended to understand the nature and incidence of the gas traced by DLAs and subDLAs.

While DLAs do contain metals (Wolfe et al. 1986; Meyer, Welty, & York 1989; Pettini, Boksenberg, & Hunstead 1990) and ionised gas (Fox et al. 2007a), they are

* Based on observations made with the William Herschel Telescope operated on the island of La Palma by the Isaac Newton Group in the Spanish Observatorio del Roque de los Muchachos of the Instituto de Astrofísica de Canarias.

characterized by low metallicities (Kulkarni et al. 2005; Akerman et al. 2005; Prochaska et al. 2007) and large neutral fractions (Viegas 1995; Vladilo et al. 2001). Little, if any, evolution is detected in the co-moving mass density of H I, Ω_{HI} , from $z \simeq 4$ to $z \approx 0.5$ (Rao, Turnshek, & Nestor, 2006; Lah et al. 2007; although see Prochaska, Herbert-Fort, & Wolfe 2005) and of metals (Kulkarni et al. 2005). This is perhaps surprising, considering the putative role of DLAs as the reservoir of fuel for star formation. In fact, recent work (Wolfe & Chen 2006; Wild, Hewett, & Pettini 2007) has shown that *in situ* star formation in DLAs is significantly less than expected on the basis of the present-day Kennicutt-Schmidt law (Kennicutt 1998), considering their large H I surface densities. One possible explanation for the apparent lack of evolution in Ω_{HI} is that a significant fraction of DLAs with high star formation rates or metallicities are missed from traditional magnitude limited optical QSO surveys due to chromatic extinction from large columns of dust. This possibility, however, is not supported by surveys of DLAs in radio-selected QSOs (Ellison et al. 2001; Jorgenson et al. 2006).

SubDLAs, on the other hand, contribute a smaller fraction of the total H I in the Universe. However, they possess larger fractions of ionised gas than DLAs, and thus the total amount of hydrogen (H I plus H II) in subDLAs may be comparable to that of DLAs (Fox et al. 2007b). Furthermore, subDLAs appear to have higher metallicities than DLAs (Kulkarni et al. 2007) and thus may be a large repository of the metals produced at high redshifts (see Pettini 2006). While DLAs and subDLAs both contain large amounts of hydrogen, they are likely to arise in different regions within galaxies and to trace different environments and properties.

Strong metal lines of Mg II $\lambda\lambda 2796, 2804$ and Fe II $\lambda\lambda 2587, 2600$ are ubiquitous in (sub)DLA systems. Their large oscillator strengths and near-ultraviolet (UV) rest wavelengths make them ideal for tracing large columns of neutral gas at redshifts $z \lesssim 1.7$, where the Ly α line falls below the atmospheric cut-off at 3200 Å and therefore requires observations from space. In this context, systems selected via strong Ca II $\lambda\lambda 3935, 3970$ absorption have recently garnered attention (Wild & Hewett 2005). Extensive literature exists on the Ca II doublet in the interstellar media of the Milky Way and nearby galaxies, since these lines can be studied from the ground even at redshift $z = 0$ (e.g. Marshall & Hobbs 1972; Welty, Morton, & Hobbs 1996 and references therein). This body of work has shown that in local interstellar environments Ca is a strongly refractory element, exhibiting some of the highest depletion factors (Savage & Sembach 1996). Furthermore, since the ionisation potential of Ca II is lower than that of hydrogen, Ca II is not the dominant ionisation stage of Ca in H I regions, unlike Mg II and Fe II. Rather, the balance between Ca II and Ca III depends on the details of the physical conditions in the gas, primarily on temperature and on the densities of particles and far-UV photons. Therefore, while all DLAs exhibit strong Mg II and Fe II lines, the same is not true of Ca II.

Wild, Hewett, & Pettini (2006; WHP06) recently conducted a survey for strong Ca II systems, with $\lambda 3935$ rest equivalent width $W_0^{\lambda 3935} \geq 0.35$ Å, in QSO spectra from the Sloan Digital Sky Survey (SDSS). Based on the strengths of Zn II and Cr II lines, WHP06 concluded that, on average, strong Ca II absorbers have $N(\text{H I})$ values above the DLA

limit. They also showed that these absorbers are, on average, dustier than typical DLAs, introducing a reddening of $\langle E(B - V) \rangle \gtrsim 0.1$ magnitudes in the spectra of the background QSOs, compared to $\langle E(B - V) \rangle \lesssim 0.02$ for the general population of SDSS DLAs (WHP06; Vladilo, Prochaska, & Wolfe 2008). This level of obscuration of the background QSOs is significant, as it causes flux-limited and/or colour-selected surveys to underestimate the numbers of strong Ca II systems. If Ca II-strong DLAs are being missed, and if they are preferentially metal-rich relative to DLAs with weaker Ca II absorption, then this class of absorption system may contain a previously overlooked repository of both neutral gas and metals. In any case, if Ca II systems select a population of absorbers with unique properties, they could hold the key to a better understanding of the detailed physical properties of DLAs and subDLAs.

Since the survey by WHP06, efforts have been devoted to better understanding the link between strong Ca II systems and galaxies. Using *K*-band imaging, Hewett & Wild (2007) reported an excess of luminous galaxies close to the sightlines to 30 QSOs with intervening Ca II systems at redshifts $0.7 < z < 1.2$. The galaxies appear to exhibit a luminosity-dependent cross section for Ca II absorption and have a mean impact parameter of ≈ 25 kpc. Together with the incidence of absorbers from WHP06, this result implies a halo volume filling factor of ~ 10 per cent out to ≈ 35 kpc from the absorbing galaxies. At lower redshifts, Zych et al. (2007) were able to associate luminous, metal-rich, star-forming spiral galaxies with four out of five strong Ca II absorbers at $z < 0.5$.

Although these studies represent progress in uncovering the nature of Ca II absorbers, ignorance of $N(\text{H I})$ in such systems limits the direct insight they provide into DLAs and subDLAs in general. While it seems very likely that Ca II absorbers select large columns of neutral gas, direct measurements of $N(\text{H I})$ are currently available for very few Ca II systems. The reason is simple: by the time the SDSS data highlighted the potential importance of absorption systems selected via Ca II, no space-borne UV spectrograph was in operation to measure the associated column densities of H I. This unfortunate state of affairs is about to change with the forthcoming installation of the Cosmic Origins Spectrograph (COS) on the refurbished *Hubble Space Telescope* (*HST*). In the meantime, the most immediate approach to this problem is to perform the complementary experiment of measuring the strength of Ca II absorption in known DLAs at redshifts $z \lesssim 1.3$, where the Ca II doublet lines are still accessible with optical spectrographs.

The samples of confirmed DLAs at these intermediate redshifts have increased considerably in recent years thanks to dedicated *HST* surveys (see Rao, Turnshek & Nestor 2006; RTN06). In this paper, we present new observations of QSOs from the RTN06 compilation designed to: (i) measure the equivalent widths of the Ca II $\lambda\lambda 3935, 3970$ doublet lines in order to assess the overlap of known DLAs (and a few subDLAs) with the strong Ca II absorber sample of WHP06; and (ii) simultaneously determine the metallicities and dust content of intermediate redshift DLAs via observations of the associated Zn II and Cr II absorption lines (Pettini et al. 1990), thereby adding to the still somewhat limited statistics of these measures at $z < 1.5$ (Akerman et al. 2005; Kulkarni et al. 2007). In Section 2 we describe our observations and

equivalent width measurements, while Section 3 deals with the derivation of column densities and element abundances. The main results on the Ca II properties of known DLAs at intermediate redshifts are presented in Section 4. We summarise our principal findings and conclusions in Section 5.

2 OBSERVATIONS AND DATA REDUCTION

2.1 Sample Selection

We selected QSOs with known DLAs and subDLAs at $0.6 < z_{\text{abs}} < 1.3$ from the compilation by RTN06. Targets were chosen on the basis of absorption redshift (so as to allow coverage of the absorption features of interest), and accessibility during the scheduled observing runs. For each target, we first examined the SDSS spectrum at the wavelengths of the expected Ca II absorption. However, those spectra have insufficient signal-to-noise ratios (S/N) and resolution to either unambiguously detect or put meaningful limits on Ca II absorption strength.

It is important to remember here that the sample assembled by RTN06 was constructed from a *targeted* Ly α survey of known Mg II absorbers. Therefore, as with any absorption line study, the manner in which systems are selected needs to be considered when interpreting the results of our survey. For example, stronger Mg II systems are exponentially less common than weaker systems (Nestor, Turnshek, & Rao 2005), but more likely to be DLAs (RTN06). Combining these two trends, one can demonstrate that the unbiased median $W_0^{\lambda 2796}$ for DLAs is $\simeq 1.35 \text{ \AA}$, compared to 1.9 \AA in our sample. Evidently, our sample is somewhat biased against DLAs with weaker Mg II absorption, compared to a blind survey.

Celestial coordinates and magnitudes for each quasar in our sample are given in Appendix A.

2.2 Observations

Observations were carried out with the ISIS double-beam spectrograph on the 4.2 m William Herschel telescope (WHT) at the Roque de Los Muchachos Observatory, La Palma, in two observing runs of three nights each, in 2006 April and 2006 November respectively. Atmospheric conditions varied from partly cloudy to clear, with seeing in the range 0.6–2.0 arcsec. In total we secured spectra of 18 QSOs covering absorption lines of 16 DLAs and six subDLAs, as detailed in Table 1.

Each observation consisted of a series of simultaneous exposures in the blue and red arms of ISIS; individual exposures typically lasted 1800 s, and the total exposure times in each arm ranged from 1 to 5.5 hours per QSO (2–3 hours in most cases). The blue arm was configured so as to cover the region encompassing the Zn II and Cr II multiplets, while the red arm was centred on the redshifted Ca II doublet. With 1200 grooves mm^{-1} gratings and a 0.8 arcsec entrance slit, ISIS delivered a spectral resolution of 0.6–0.7 \AA full width at half maximum (FWHM), sampled with three pixels of the EEV (blue arm) and Marconi (red arm) CCDs. Bright B-type stars were observed each night to provide templates for the removal of telluric absorption lines. The emission line spectra of hollow-cathode Cu-Ar and Cu-Ne lamps were

recorded at hourly intervals to be used for subsequent wavelength calibration. Spectrophotometric standards from the compilation by Massey et al. (1988) allowed for flux calibration of the QSO spectra.

2.3 Data Reduction and Measurements

The reduction of the two-dimensional images into co-added one-dimensional spectra followed standard procedures. We used IRAF¹ scripts to carry out the initial stages of bias subtraction, flat-fielding, wavelength calibration, background subtraction, and spectral extraction. The individual spectra of each QSO were co-added with weights proportional to the S/N and then binned onto a linear, vacuum heliocentric wavelength scale with approximately three bins per resolution element. The final steps in the data reduction involved correction for telluric absorption (if it occurred close to absorption lines of interest), and normalisation of each spectrum to the local QSO continuum.

In Figures 1 and 2 we have reproduced normalised portions of the spectra encompassing the Zn II, Cr II and Ca II absorption lines in, respectively, the 16 DLAs and six subDLAs, ordered in increasing Right Ascension. As can be appreciated from inspection of these two figures, the S/N achieved differs significantly from QSO to QSO, depending on the variable sky transparency, seeing, QSO magnitude and redshifted wavelengths of the features of interest. In every case, however, the combination of S/N and spectral resolution is sufficient to detect a Ca II $\lambda 3935$ absorption line with a rest equivalent width $W_0^{\lambda 3935} = 0.35 \text{ \AA}$ (the threshold of the SDSS survey by WHP06) at the $\geq 5\sigma$ significance level.

Values of the $W_0^{\lambda 3935}$ are listed in column (5) of Table 1; 3σ upper limits are given for cases where no Ca II absorption could be identified. We detected the stronger member of the Ca II doublet, $\lambda 3935$, in 12 out of the 16 DLAs targeted; however, only four of the DLAs meet the selection criterion $W_0^{\lambda 3935} \geq 0.35 \text{ \AA}$ of the survey by WHP06. We return to this point in Section 4 below. For reference, we also give in column (4) of Table 1 the rest-frame equivalent width of the stronger member of the Mg II doublet, $W_0^{\lambda 2796}$, from the work by RTN06.

While this study represents the first systematic study of Ca II absorption in (sub)DLAs, UV absorption lines in many of the systems in our sample have previously been studied by other authors. However, for five of the 16 DLAs and one of the six subDLAs, no previous measurements of the abundances of Zn and Cr have been reported. For four other systems, improved data for Zn and Cr are reported, two of which are significant and two which are marginal improvements over published results. Cases where the previous measurements are of superior precision to ours are indicated by notes in columns (7) and (8) of Table 1.

As well as considering the individual spectra, we also constructed stacked spectra by adding together the normalised spectra of each DLA in the Zn II-Cr II and Ca II

¹ IRAF is distributed by the National Optical Astronomy Observatories, which are operated by the Association of Universities for Research in Astronomy, Inc. under cooperative agreement with the National Science Foundation.

Table 1. DLAs OBSERVED, EQUIVALENT WIDTHS, COLUMN DENSITIES, AND ABUNDANCES

| QSO | z_{em} | z_{abs} | $W_0^{\lambda 2796}$ (Å) | $W_0^{\lambda 3935}$ (Å) | $\log N(\text{H I})$ (cm^{-2}) | $\log N(\text{Zn II})$ (cm^{-2}) | $\log N(\text{Cr II})$ (cm^{-2}) | [Zn/H] | [Cr/Zn] |
|-----------|-----------------|------------------|-----------------------------|-----------------------------|--|--|--|-----------------------------|-----------------------------|
| (1) | (2) | (3) | (4) | (5) | (6) | (7) | (8) | (9) | (10) |
| 0139–0023 | 1.384 | 0.6825 | 1.24 | 0.24 ± 0.03 | $20.60^{+0.05}_{-0.12}$ | < 13.15 | < 13.66 | < -0.08 | ... |
| 0253+0107 | 1.035 | 0.6316 | 2.57 | 0.46 ± 0.04 | $20.78^{+0.12}_{-0.08}$ | < 13.06 | < 13.69 | < -0.35 | ... |
| 0256+0110 | 1.349 | 0.7252 | 3.10 | 0.39 ± 0.04 | $20.70^{+0.11}_{-0.22}$ | $13.20 \pm 0.09^{\text{a}}$ | $12.72 \pm 0.68^{\text{a}}$ | $-0.13 \pm 0.24^{\text{a}}$ | $-1.50 \pm 0.68^{\text{a}}$ |
| 0449–168 | 2.679 | 1.0072 | 2.14 | < 0.04 | $20.98^{+0.06}_{-0.07}$ | $(12.62 \pm 0.07)^{\dagger}$ | $(13.47 \pm 0.02)^{\dagger}$ | -0.99 ± 0.10 | -0.17 ± 0.07 |
| 0454+039 | 1.343 | 0.8591 | 1.45 | 0.063 ± 0.008 | 20.67 ± 0.03 | 12.42 ± 0.06 | 13.44 ± 0.02 | -0.88 ± 0.06 | $+0.00 \pm 0.06$ |
| 1007+0042 | 1.681 | 1.0373 | 2.98 | < 0.08 | $21.15^{+0.15}_{-0.24}$ | 13.27 ± 0.04 | 13.55 ± 0.08 | -0.51 ± 0.24 | -0.74 ± 0.09 |
| 1009–0026 | 1.244 | 0.8426 | 0.71 | < 0.05 | $20.20^{+0.05}_{-0.06}$ | $< 12.36^{\text{b}}$ | $< 13.11^{\text{b}}$ | $< -0.47^{\text{b}}$ | ... |
| | | 0.8860 | 1.90 | 0.07 ± 0.02 | $19.48^{+0.01}_{-0.08}$ | $12.43 \pm 0.14^{\text{b}}$ | $< 13.10^{\text{b}}$ | $0.32 \pm 0.15^{\text{b}}$ | $< -0.35^{\text{b}}$ |
| 1010+0003 | 1.399 | 1.2642 | 1.12 | 0.26 ± 0.02 | $21.52^{+0.06}_{-0.07}$ | 13.01 ± 0.02 | 13.69 ± 0.02 | -1.14 ± 0.07 | -0.34 ± 0.03 |
| 1107+0048 | 1.392 | 0.7402 | 2.95 | 0.34 ± 0.01 | $21.00^{+0.02}_{-0.05}$ | 13.12 ± 0.04 | 13.75 ± 0.04 | -0.52 ± 0.07 | -0.39 ± 0.06 |
| 1107+0003 | 1.740 | 0.9542 | 1.36 | 0.26 ± 0.02 | $20.26^{+0.09}_{-0.14}$ | $< 12.38^{\text{c}}$ | $< 13.18^{\text{c}}$ | $< -0.51^{\text{c}}$ | ... |
| 1220–0040 | 1.411 | 0.9746 | 1.95 | < 0.08 | $20.20^{+0.05}_{-0.09}$ | $< 12.55^{\text{d}}$ | $< 13.11^{\text{d}}$ | $< -0.28^{\text{d}}$ | ... |
| 1224+0037 | 1.482 | 1.2346 | 1.09 | < 0.16 | $20.88^{+0.04}_{-0.09}$ | $< 12.61^{\text{b}}$ | $< 13.30^{\text{b}}$ | $< -0.90^{\text{b}}$ | ... |
| | | 1.2665 | 2.09 | < 0.15 | $20.00^{+0.08}_{-0.05}$ | $< 12.62^{\text{b}}$ | $< 13.03^{\text{b}}$ | $< -0.01^{\text{b}}$ | ... |
| 1225+0035 | 1.226 | 0.7728 | 1.74 | 0.36 ± 0.03 | $21.38^{+0.11}_{-0.12}$ | 13.23 ± 0.07 | 13.81 ± 0.06 | -0.78 ± 0.14 | -0.44 ± 0.09 |
| 1323–0021 | 1.390 | 0.7156 | 2.23 | 0.82 ± 0.02 | 20.54 ± 0.15 | $13.29 \pm 0.21^{\text{a}}$ | 13.70 ± 0.18 | $+0.12 \pm 0.26$ | -0.61 ± 0.28 |
| 1727+5302 | 1.444 | 0.9445 | 2.83 | 0.29 ± 0.03 | $21.16^{+0.04}_{-0.05}$ | 13.23 ± 0.03 | 13.80 ± 0.03 | -0.56 ± 0.06 | -0.45 ± 0.04 |
| | | 1.0306 | 0.92 | 0.16 ± 0.02 | 21.41 ± 0.03 | $12.68 \pm 0.07^{\text{e}}$ | $13.36 \pm 0.06^{\text{e}}$ | $-1.36 \pm 0.08^{\text{e}}$ | $-0.34 \pm 0.09^{\text{e}}$ |
| 1733+5533 | 1.072 | 0.9981 | 2.17 | < 0.07 | $20.70^{+0.04}_{-0.03}$ | 12.89 ± 0.06 | 13.34 ± 0.07 | -0.44 ± 0.07 | -0.57 ± 0.09 |
| 2149+212 | 1.538 | 0.9111 | 0.72 | 0.12 ± 0.01 | $20.70^{+0.08}_{-0.10}$ | < 12.40 | < 12.78 | < -0.93 | ... |
| | | 1.0023 | 2.46 | < 0.11 | $19.30^{+0.02}_{-0.05}$ | < 12.13 | < 12.59 | $< +0.20$ | ... |
| 2353–0028 | 0.765 | 0.6043 | 1.60 | 0.17 ± 0.03 | 21.54 ± 0.15 | 13.25 ± 0.29 | 13.40 ± 0.17 | -0.92 ± 0.32 | -0.86 ± 0.33 |

\dagger from Péroux et al. (2008). Measurements having greater precision are reported by: (a) Péroux et al. (2006a); (b) Meiring et al. (2007); (c) Meiring et al. (2006); (d) Meiring et al. (2008); (e) Khare et al. (2004).

Table 2. MEASUREMENTS FROM THE LITERATURE

| QSO | z_{em} | z_{abs} | $W_0^{\lambda 2796}$ (Å) | $W_0^{\lambda 3935}$ (Å) | $\log N(\text{H I})$ (cm^{-2}) | $\log N(\text{Zn II})$ (cm^{-2}) | $\log N(\text{Cr II})$ (cm^{-2}) | [Zn/H] | [Cr/Zn] | Ref. ^b |
|-----------|-----------------|------------------|-----------------------------|-----------------------------|--|--|--|------------------|------------------|-------------------|
| (1) | (2) | (3) | (4) | (5) | (6) | (7) | (8) | (9) | (10) | (11) |
| 0515–4414 | 1.713 | 1.1508 | 2.34 | 0.36 ± 0.07 | 19.88 ± 0.05 | 12.18 ± 0.02 | 12.48 ± 0.04 | -0.33 ± 0.05 | -0.72 ± 0.04 | 1,2 |
| 0738+313 | 0.630 | 0.0912 | ... | 0.19 ± 0.01 | $21.18^{+0.05}_{-0.07}$ | < 12.662 | 13.28 ± 0.22 | < -1.15 | > -0.40 | 3 |
| 0738+313 | 0.630 | 0.2210 | 0.61 | 0.06 ± 0.01 | $20.90^{+0.07}_{-0.08}$ | < 12.825 | 13.11 ± 0.24 | < -0.71 | > -0.74 | 3 |
| 1436–0051 | 1.275 | 0.7377 | 1.11 | 0.40 ± 0.02 | $20.08^{+0.10}_{-0.12}$ | 12.67 ± 0.05 | < 12.71 | -0.04 ± 0.12 | < -0.98 | 4 |
| 2328+0022 | 1.309 | 0.652 | 1.90 | 0.24 ± 0.02 | $20.32^{+0.06}_{-0.07}$ | 12.43 ± 0.15 | 13.35 ± 0.19 | -0.52 ± 0.22 | -0.10 ± 0.24 | 5 |
| 2331+0038 | 1.486 | 1.1414 | 2.53 | 0.26 ± 0.02 | $20.00^{+0.04}_{-0.05}$ | 12.22 ± 0.09 | < 12.37 | -0.41 ± 0.12 | < -0.87 | 6 |
| 2335+1501 | 0.790 | 0.6798 | 0.97 | 0.19 ± 0.03 | $19.70^{+0.30}_{-0.30}$ | 12.37 ± 0.04 | 12.89 ± 0.10 | $+0.04 \pm 0.30$ | -0.50 ± 0.11 | 7 |

^bReferences—1: de la Varga et al. (2000); 2: Quast et al. (2008); 3: Meiring et al. (2006); 4: Meiring et al. (2008); 5: Péroux et al. (2006a); 6: Meiring et al. (2007); 7: Péroux et al. (2008).

regions (in the DLA rest frame), following the same procedure as WHP06. The resulting average spectrum, which includes DLAs in which the Ca II lines are below our detection limit, is useful for comparative studies, as discussed below. A second average spectrum was assembled by adding together the data for each subDLA. The borderline DLA towards 1107+0003 ($\log N(\text{H I}) = 20.26 \pm 0.1$) was included in the DLA stack; the inclusion/exclusion of this system in the DLA/subDLA stack has little effect on the results. The Zn II–Cr II region of the DLA towards 0449–168 was excluded from all stacks, as it falls within the Ly α forest (see Figure 1).

3 COLUMN DENSITIES AND ELEMENT ABUNDANCES

Column densities of Zn II and Cr II were measured by fitting the observed absorption lines with theoretical profiles generated with the software package vPFIT² as described, for example, by Rix et al. (2007). Briefly, vPFIT uses χ^2 minimisation to deduce the values of redshift z , column density N (cm^{-2}), and Doppler parameter b (km s^{-1}) that best reproduce the observed absorption line profiles. vPFIT takes

² vPFIT is available from <http://www.ast.cam.ac.uk/~rfc/vpfit.html>

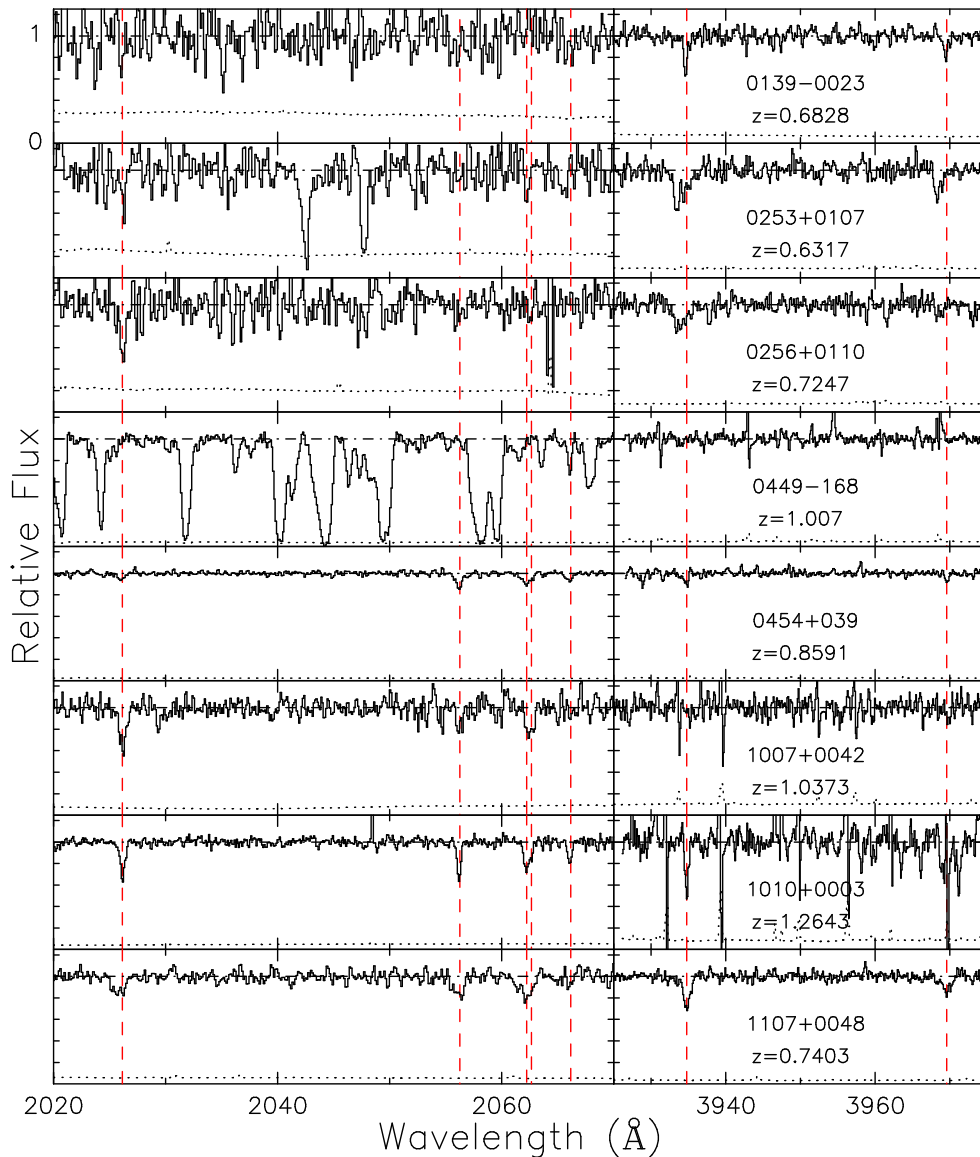
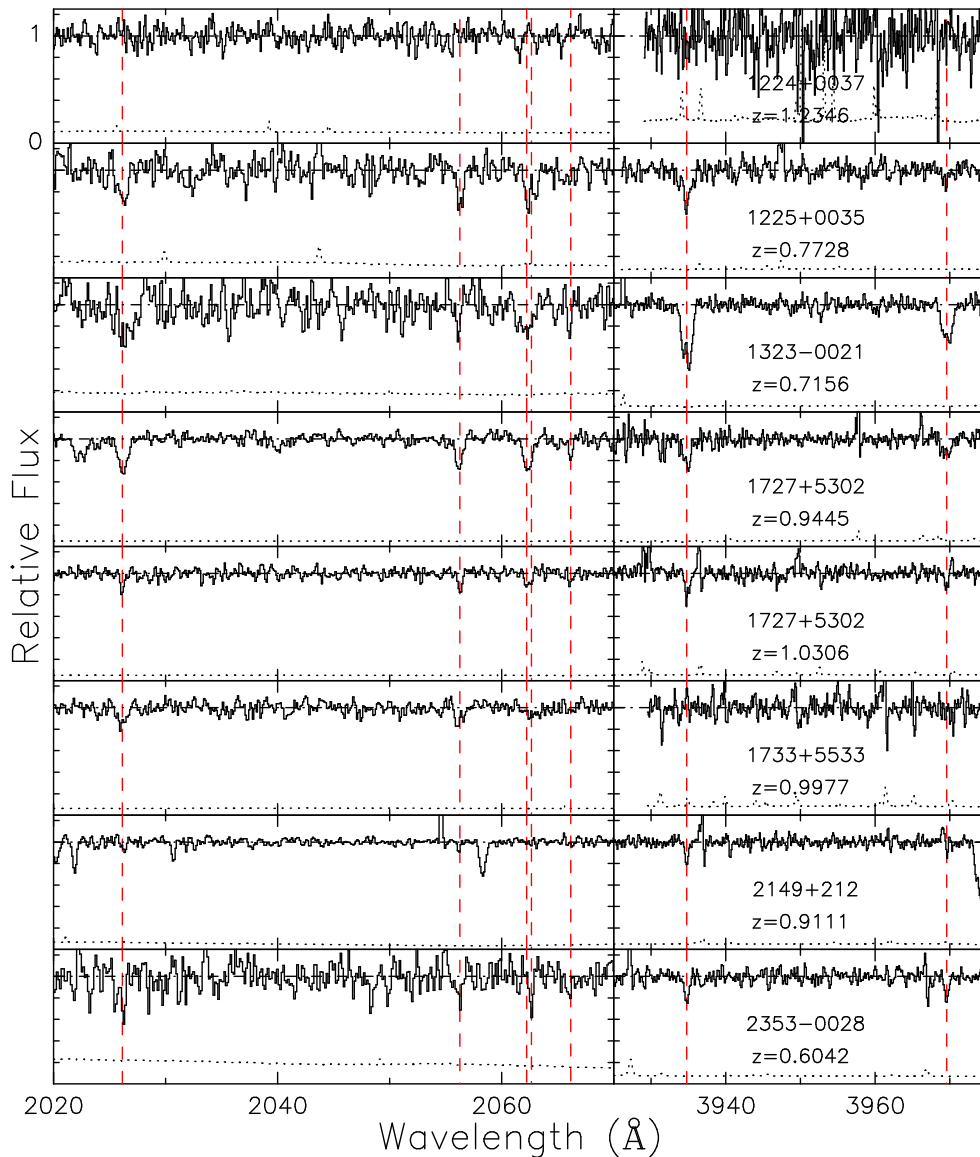


Figure 1. The Zn II–Cr II (left) and Ca II (right) regions of the spectra of the 16 DLAs observed. The spectra have been normalised to the underlying QSO continuum and reduced to the rest frame of the DLA. In each panel, the horizontal dash-dot line indicates the continuum level, while the dotted line near the bottom of each plot shows the 1σ error spectrum. Vertical long-dash lines are drawn at the wavelengths of the Zn II $\lambda\lambda 2026, 2063$ doublet, Cr II $\lambda\lambda 2056, 2062, 2066$ triplet, and Ca II $\lambda\lambda 3935, 3970$ doublet.

into account the instrumental broadening function in its χ^2 minimisation and error evaluation. Laboratory (vacuum) wavelengths and f -values of the transitions analysed were taken from the compilation by Morton (2003) with subsequent updates by Jenkins & Tripp (2006). In most cases, the resolution of our spectra ($\text{FWHM} \approx 30\text{--}60 \text{ km s}^{-1}$) is insufficient to resolve the intrinsic velocity structure of the gas. However, as we are dealing with weak absorption lines, we do not expect line saturation to be a problem (see the discussion by Pettini et al. 1990); the measured doublet (Zn II) and triplet (Cr II) ratios confirm that this is indeed the case for the systems analysed here.

Values of $N(\text{Zn II})$ and $N(\text{Cr II})$ are listed in Table 1, together with the errors estimated by VPFIT on the basis of the S/N ratios of the spectra. Since these species are the dominant ionisation stages of Zn and Cr in HI regions

(e.g. Morton et al. 1973; Viegas 1995), the corresponding element abundances can be inferred directly from the ratios $N(\text{Zn II})/N(\text{H I})$ and $N(\text{Cr II})/N(\text{H I})$. Values of $N(\text{H I})$ for the systems observed are reproduced in column (6) of Table 1 from the compilation by RTN06. Reference to the solar values of Zn/H and Cr/Zn ($\log(\text{Zn}/\text{H})_{\odot} = -7.37$ and $\log(\text{Cr}/\text{Zn})_{\odot} = +1.02$; Lodders 2003), then gives the quantities $[\text{Zn}/\text{H}]$ and $[\text{Cr}/\text{Zn}]$ in the usual definition $[X/Y] \equiv \log(X/Y)_{\text{DLA}} - \log(X/Y)_{\odot}$. The former is often adopted as a measure of the metallicity, while the latter provides an indication of the degree of dust depletion of refractory elements, for the reasons discussed by Pettini et al. (1990). Values of $[\text{Zn}/\text{H}]$ and $[\text{Cr}/\text{Zn}]$ for the systems observed are given in the last two columns of Table 1; the errors quoted were obtained by combining in quadrature the errors on the column densities of the respective ions.

Figure 1. (*cont'd*)

As noted above, measurements of Zn and Cr abundances have been previously reported in the literature for many of the absorbers in our sample. Out of the ten DLAs in common with previous work for which we have estimates of $[\text{Zn}/\text{H}]$ and $[\text{Cr}/\text{Zn}]$, eight are in very good agreement with published values. The exceptions are the DLAs in the spectra of the QSOs 1225+0035 and 1733+5533 (at $z_{\text{abs}} = 0.7728$ and 0.9981 respectively) where the values of $[\text{Zn}/\text{H}]$ implied from our detections of the Zn II doublet lines (see Figure 1) are actually higher than the upper limits estimated by Meiring et al. (2006). However, these authors' data are of rather poor S/N at the relevant wavelengths.

3.1 Metallicity Evolution of DLAs

The most recent compilation of $[\text{Zn}/\text{H}]$ measurements in DLAs by Kulkarni et al. (2007) includes 18 systems in the redshift range $0.6 < z < 1.3$ (corresponding to a time inter-

val amounting to nearly one quarter of the current age of the universe). Thus, the five new (and two improved) measurements reported here constitute a significant addition to the DLA statistics at these epochs. In Figure 3 we plot the full sample of $[\text{Zn}/\text{H}]$ measurements as a function of redshift. The new/improved data reported here, shown with solid squares, confirm the wide range of metallicities exhibited by DLAs *at all redshifts*: as pointed out by Pettini et al. (1994, 1997b), at any one epoch DLA metallicities can span two orders of magnitude, from nearly solar to $\sim 1/100$ of solar.

Also shown in Figure 3 are the mean values of the column density-weighted metallicity, $[\langle \text{Zn}/\text{H} \rangle]$ (where $\langle \text{Zn}/\text{H} \rangle = \sum N(\text{Zn II}) / \sum N(\text{H I})$ —see Pettini et al. 1994), for the redshift range of our sample ($0.6 < z_{\text{abs}} < 1.3$) and for higher redshift DLAs in two bins: $1.3 < z_{\text{abs}} < 2.6$ and $2.6 < z_{\text{abs}} < 4$. As discussed by Kulkarni et al. (2007 and references therein), there is evidence for mild evolution of the mean DLA metallicity with the progress of time, in the

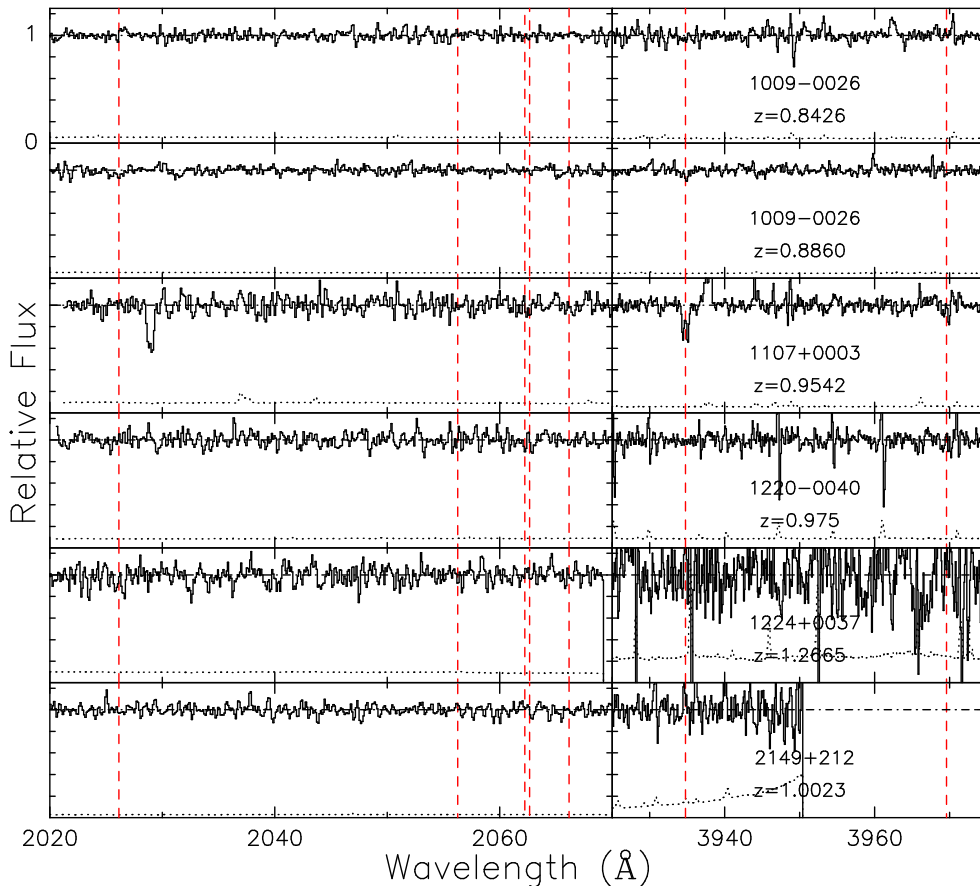


Figure 2. As in Figure 1, but for the six subDLAs observed.

sense that the value $[\langle \text{Zn}/\text{H} \rangle] = -0.71 \pm 0.08$ we measure at $0.6 < z_{\text{abs}} \leq 1.3$ is a factor of about two to three higher than in the other two redshift bins: $[\langle \text{Zn}/\text{H} \rangle] = -1.06 \pm 0.06$ at $1.3 < z_{\text{abs}} \leq 2.6$, and $[\langle \text{Zn}/\text{H} \rangle] = -1.14 \pm 0.11$ at $2.6 < z_{\text{abs}} \leq 4.0$, respectively.

One of the factors which affect this type of comparison, and yet is generally overlooked, is the fact that DLAs with $z_{\text{abs}} < 1.7$ are normally selected via their (strong) $\text{Mg II } \lambda 2796$ absorption, while the selection at higher redshifts is via the damped $\text{Ly}\alpha$ line itself. The two criteria may not be equivalent; in particular, it now seems well established that DLAs with strong Mg II absorption are on the whole more metal-rich than the average (Nestor et al. 2003; Murphy et al. 2007). To assess the importance of this potential bias, we use four distributions: (i) the distribution of DLA metallicities as a function of $W_0^{\lambda 2796}$ – at redshifts $0.6 < z < 1.3$, we find that $[\text{Zn}/\text{H}] \propto (W_0^{\lambda 2796})^{1.7 \pm 0.1}$ is a good representation of the 12 measured values in our sample (Pearson’s $r = 0.85 \pm 0.08$, $\chi^2_\nu = 2.7$); (ii) the DLA fraction as a function of $W_0^{\lambda 2796}$ from RTN06; (iii) the distribution of values of $W_0^{\lambda 2796}$ in SDSS QSOs from Nestor et al. (2005); and (iv) the distribution of values of $W_0^{\lambda 2796}$ in the sample used to estimate $[\langle \text{Zn}/\text{H} \rangle]$, to arrive at the conclusion that the value of $[\langle \text{Zn}/\text{H} \rangle] = -0.7 \pm 0.08$ at $0.6 < z_{\text{abs}} < 1.3$ is probably biased too high by ~ 0.1 dex. Although this is not a large factor, it nevertheless dilutes further the evidence for redshift evolution of the mean metallicity of DLAs.

3.2 Depletion of Chromium

In Figure 4 we have plotted $[\text{Cr}/\text{Zn}]$ as a function of DLA metallicity (as measured by the $[\text{Zn}/\text{H}]$ ratio), again combining the systems in the compilation by Kulkarni et al. (2007) with the new, or improved, measurements from the present work. Both Zn and Cr track the abundance of Fe in Galactic stars with $[\text{Fe}/\text{H}] \gtrsim -2$ (i.e. in the same metallicity regime as the vast majority of DLAs—see Cayrel et al. 2004 and Nissen et al. 2007). On the other hand, in the ISM near the Sun, Cr is among the most depleted elements with only a small fraction in the gas phase while most of it is ‘hidden away’ in dust grains; Zn, on the contrary, exhibits at most only mild depletions (Savage & Sembach 1996). Thus, the $[\text{Cr}/\text{Zn}]$ ratio in DLAs is a convenient way to assess the degree to which refractory elements are depleted in the ISM of the galaxies hosting these absorbers (Pettini et al. 1990) and, by inference, obtain an indication of their dust content (Pettini et al. 1997a).

In Figure 4 we see the clear correlation between Cr depletion and metallicity that has already been noted (e.g. Pettini et al. 1994; Ledoux, Petitjean & Srianand 2003; Akerman et al. 2005; Meiring et al. 2006); the data reported here fit the known trend and improve the statistics at the high metallicity end. Although the measurements scatter about the mean relation between Cr depletion and Zn abundance, the data in Figure 4 show that in DLAs with metallicities $[\text{Zn}/\text{H}] \lesssim -1.5$, Cr suffers little depletion relative to Zn;

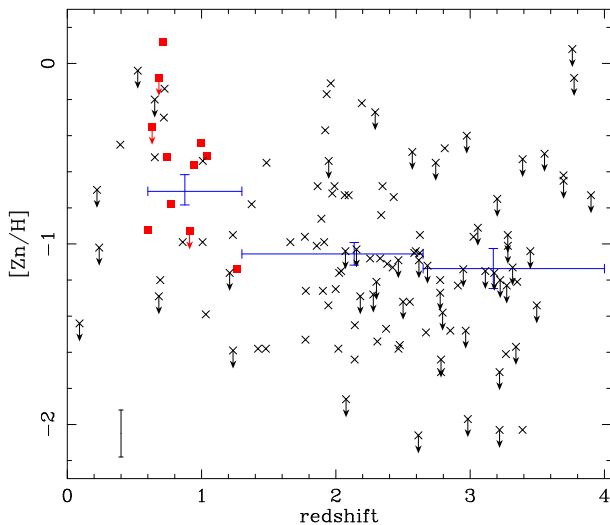


Figure 3. Measurements of $[Zn/H]$ in DLAs at $0 < z_{\text{abs}} < 4$ from the compilation by Kulkarni et al. (2007) and from the present work. Except for the cases in which there exists a superior measurement in the literature, the DLAs from the present study are shown as red squares. Upper-limits are indicated with downward pointing arrows. Also shown are the mean values of column density-weighted metallicity $[\langle Zn/H \rangle]$ (see text for definition) in three redshift intervals, together with the $\pm 1\sigma$ ranges calculated via bootstrap techniques. As discussed in the text, the value of $[\langle Zn/H \rangle]$ at $0.6 < z_{\text{abs}} \leq 1.3$ may be biased too high by about 0.1 dex, because these DLAs were primarily selected by their strong Mg II absorption. The vertical bar in the lower left-hand corner gives an indication of the typical error in $[Zn/H]$.

on the other hand, in the DLAs with near-solar metallicities, ~ 75 per cent of the Cr is presumably incorporated into dust ($[Cr/Zn] \simeq -0.6$). This is still a relatively modest degree of depletion compared to that exhibited by Cr in diffuse clouds in the Milky Way disk, and more akin to the values seen along sight-lines which sample mostly the interstellar medium in the halo of our Galaxy (see Figure 6 of Savage & Sembach 1996). The origin and implications of this metallicity-dependent depletion pattern have been considered by Vladilo (2002).

4 CA II ABSORPTION IN DLAS

A primary aim of the observations presented in this paper is to establish the Ca II content of known DLAs at intermediate redshifts. Ultimately, we hope to clarify the relationship between absorbers with strong Ca II lines, which can be selected from ground-based QSO spectra such as those from the SDSS without reference to the Ly α line, and the more general population of DLAs.

For the reasons discussed by WHP06, we suspect that strong Ca II absorbers may be a subset of the DLA population. However, the properties of DLAs that lead to strong Ca II absorption are not clear. WHP06 considered three possibilities; they proposed that strong Ca II absorbers select DLAs with: (i) the largest $N(\text{H I})$ values; (ii) the highest metallicities; or (iii) the largest volume densities, $n(\text{H}_{\text{TOT}})$. A further possibility is an absence or destruction of dust grains, leading to unexpectedly large fractions of Ca atoms

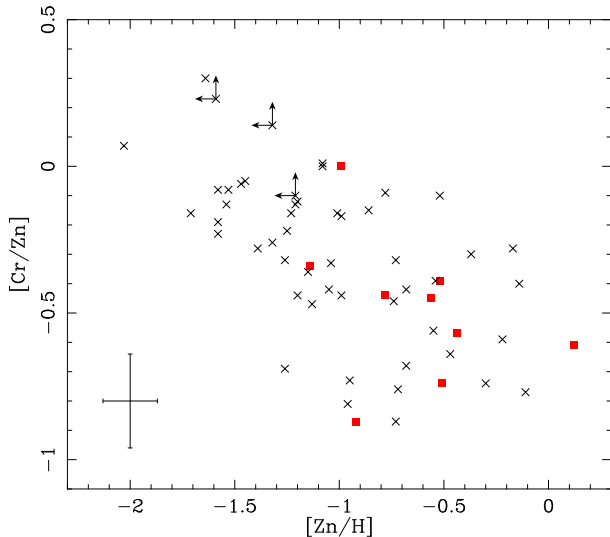


Figure 4. Measurements of $[Cr/Zn]$ in DLAs from the compilation by Kulkarni et al. (2007) and from the present work. DLAs from the present work are shown by red squares unless a superior measurement exists in the literature. The error bars in the lower left-hand corner show the typical uncertainties in the ratios plotted.

in the gas phase (although this would be in contradiction to the finding that strong Ca II absorbers induce higher-than-average reddening in the background quasar). We now consider these possibilities in turn, in light of the new data presented here.

4.1 Ca II as a Tracer of Column Density?

We examine in Figure 5 the relationship between the equivalent width of the stronger member of the Ca II doublet, $W_0^{\lambda 3935}$, and the column density of neutral hydrogen $N(\text{H I})$. We have augmented our sample with a trawl of the literature for other measurements of Ca II in DLAs and subDLAs, collected in Table 2. However, it must be borne in mind that the six additional systems thus found do not represent a statistical sample, because non-detections of Ca II and the corresponding upper limits on $W_0^{\lambda 3935}$ generally go unreported in the literature.

The data collected in Figure 5 do not support the hypothesis that strong Ca II absorption corresponds exclusively to DLAs at the upper end of the $N(\text{H I})$ distribution. WHP06 showed that, if this were the case, the incidence of strong Ca II absorbers per unit redshift would match that of DLAs with $10^{21} \lesssim N(\text{H I}) \lesssim 10^{22}$ so that, in this scenario, the former would account for all of the latter. In contrast, our combined sample includes eight DLAs with $N(\text{H I}) \geq 10^{21}$, and *none* of them is a strong Ca II absorber.

More generally, inspection of Figure 5 shows that there is no simple relation between $W_0^{\lambda 3935}$ and $N(\text{H I})$ in DLAs. Selecting absorption systems by Ca II equivalent width does, however, primarily select DLAs: among the systems we have observed, all those with $W_0^{\lambda 3935} > 0.15 \text{ \AA}$ are DLAs [within the accuracy of the determination of $N(\text{H I})$]. On the other hand, there are subDLAs with $W_0^{\lambda 3935} > 0.15 \text{ \AA}$ reported in the literature. Conversely, selecting by $N(\text{H I})$ does not ensure that a strong Ca II line is present: over one third

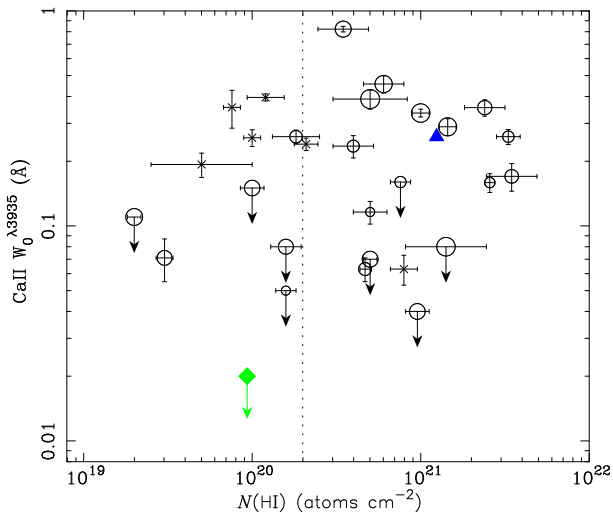


Figure 5. The rest-frame equivalent width of the Ca II $\lambda 3935$ line plotted as a function of the column density of neutral hydrogen. *Open circles:* DLAs from the present survey; the size of the circle is proportional to the equivalent width of Mg II $\lambda 2796$ ($0.7 \text{ \AA} < W_0^{\lambda 2796} < 3.1 \text{ \AA}$ — see Table 1). Upper limits to $W_0^{\lambda 3935}$ are 3σ . *Crosses:* additional measurements from the literature (listed in Table 2). Note, however, that these are likely to be biased towards higher-than-average values of $W_0^{\lambda 3935}$. *Filled (blue) triangle and filled (green) diamond:* values measured from the stacked spectra of, respectively, the DLAs and sub-DLAs in Table 1, plotted at the corresponding mean values of $N(\text{H I})$ (see section 2.3). The vertical dash line shows the conventional distinction between DLAs and subDLAs at $N(\text{H I}) = 2 \times 10^{20} \text{ cm}^{-2}$.

of the DLAs in our sample have $W_0^{\lambda 3935} < 0.15 \text{ \AA}$ and three quarters have $W_0^{\lambda 3935} < 0.3 \text{ \AA}$. On the basis of our composite spectrum (blue triangle in Figure 5 — see section 2.3), we conclude that Ca II absorption with an average $\langle W_0^{\lambda 3935} \rangle = 0.26 \text{ \AA}$ is associated with known DLAs. Furthermore, despite the few strong detections reported in the literature, the composite spectrum of the sub-DLAs in our sample shows that their associated Ca II absorption is weak, with an average $\langle W_0^{\lambda 3935} \rangle < 0.02 \text{ \AA}$ (green diamond in Figure 5).

We note that only four out of the 19 DLAs in the combined sample meet the selection criterion $W_0^{\lambda 3935} \geq 0.35 \text{ \AA}$ of the SDSS survey by WHP06, and only *one* out of 19 would be classed as a ‘strong’ Ca II absorber ($W_0^{\lambda 3935} \geq 0.5 \text{ \AA}$) by WHP06. Evidently, there is little overlap as yet between confirmed DLAs and the SDSS candidates identified via Ca II. This is not surprising, however, when we consider the magnitude limit of the *HST* observations which RTN06 used to assemble the current sample of intermediate redshift DLAs.

Specifically, WHP06 estimate that the true (unbiased) redshift path density of Ca II with $W_0^{\lambda 3935} > 0.5 \text{ \AA}$ is ~ 20 – 30 per cent of that of DLAs. However, for a flux-limited sample in the SDSS *i*-band they also calculate that ~ 40 per cent of their strong Ca II systems are missed due to the relatively strong extinction of the background QSOs by such absorbers. A detailed description of the calculation is provided in Section 6.1 of WHP06. The majority of quasars included in the RTN06 compilation were discovered either using much bluer passbands (usually *B* or *V*), or from an SDSS *g*-band flux-limited sample. The fractional loss of

strong Ca II-systems from the RTN06 compilation may be calculated using exactly the same procedure as described in WHP06 but using observed-frame wavelengths appropriate for the *B*-, *V*- or *g*-bands instead of the $\sim 8000 \text{ \AA}$ SDSS *i*-band. The significantly shorter absorber rest-frame wavelengths probed by the bluer passbands mean that the fraction of background QSOs falling below a pre-defined flux-limit increases to ~ 80 per cent, compared to the ~ 40 per cent loss for the SDSS *i*-band. Assuming that $N(\text{H I})$ and $W_0^{\lambda 3935}$ are unrelated in DLAs, we thus calculate that our sample of 16 DLAs was likely to include only one Ca II-absorber with $W_0^{\lambda 3935} > 0.5 \text{ \AA}$, as indeed turned out to be the case (the $W_0^{\lambda 3935} = 0.82 \text{ \AA}$ absorber at $z_{\text{abs}} = 0.7156$ towards 1323–0021). Estimates of the degree of reddening for individual absorbers in our sample are given in Appendix A.

Returning to Figure 5, it can also be appreciated that there is no obvious correlation between $W_0^{\lambda 3935}$ and Mg II $W_0^{\lambda 2796}$ — the size of the open circles in the Figure is proportional to the latter quantity. Mg II absorption in DLAs is typically at least moderately saturated and, thus, primarily a tracer of the velocity structure of the absorbing gas.

4.2 Ca II as a Tracer of Metallicity or Dust Content?

We have searched for other clues to the origin of strong Ca II absorbers by testing for correlations of $W_0^{\lambda 3935}$ with DLA metallicity (as measured by $[\text{Zn}/\text{H}]$) and dust depletions (via $[\text{Cr}/\text{Zn}]$, as explained in Section 3.2 above). As can be seen from Figure 6, no such correlation with $[\text{Zn}/\text{H}]$ is evident in the present data set. The only DLA in our sample with $W_0^{\lambda 3935} > 0.5 \text{ \AA}$ is indeed the most metal-rich known at any redshift³, with $[\text{Zn}/\text{H}] = +0.12 \pm 0.26$ (see Figures 6 and 3). However, DLAs with $W_0^{\lambda 3935} \gtrsim 0.15 \text{ \AA}$ span essentially the full range of values of $[\text{Zn}/\text{H}]$. Due to the dearth of strong Ca II absorbers in our sample, it is difficult to test the hypothesis that the strongest Ca II absorbers represent the DLAs with the highest metallicities. However, the highly-enriched nature of the lone strong Ca II absorber in our survey suggests that metallicity may play some role.

Given the highly refractory nature of Ca, we also consider whether a lack of dust grains, leading to a large fraction of Ca remaining in the gas phase, may be an important factor in determining Ca II absorption strength. However, Figure 7 shows no obvious relationship between Ca II absorption and depletion of Cr present. The values of $[\text{Cr}/\text{Zn}]$ determined here are similar to those of other DLA samples and, in particular, we find no evidence for higher values of $W_0^{\lambda 3935}$ in DLAs with low dust depletions (as evidenced by near-solar values of $[\text{Cr}/\text{Zn}]$). The lone strong Ca II absorber in our sample has a $[\text{Cr}/\text{Zn}]$ value consistent with the average for systems of similar Ca II-strength reported by WHP06.

³ This system is discussed by Péroux et al. (2006b) as a subDLA based on the $N(\text{H I})$ measurement of Khare et al. (2004). However, we use the subsequent measurement by Rao, Turnshek and Nestor (2006) of $N(\text{H I}) = 20.54 \pm 0.15$.

4.3 Ca II as a Tracer of Volume Density?

The strengths of Mg II, Zn II, and Cr II lines in DLAs are determined primarily by the H I column density, metallicity, and dust depletion, as well as the velocity dispersion of the gas and the oscillator strengths of the transitions. This is because these ions are the dominant species of Mg, Zn, and Cr in H I regions, where photons with sufficient energy to ionise these elements beyond their first ions do not penetrate. The same is not true of Ca II. With an ionisation potential of 11.87 eV, a significant fraction of Ca can be doubly ionised even when the bulk of the gas is neutral. In photoionisation equilibrium, the balance between doubly and singly ionised Ca is given by:

$$\frac{n(\text{Ca}^{2+})}{n(\text{Ca}^+)} = \frac{\Gamma}{\alpha(T)n(e)} \quad (1)$$

where n denotes volume densities, Γ is the Ca^+ photoionisation rate, $\alpha(T)$ is the recombination coefficient to form Ca^+ , and $n(e)$ is the electron density. Presumably, this dependence of $n(\text{Ca}^{2+})/n(\text{Ca}_{\text{TOT}})$ on the local physical conditions is the extra factor responsible for the lack of any obvious correlation of $W_0^{\lambda 3935}$ with H I column density, metallicity and depletion levels.

We can exploit this feature of Ca II absorbers to gain information on the physical conditions which determine the ionisation balance of Ca. Since we know, or have estimates of, $N(\text{H I})$, metallicity (from $[\text{Zn}/\text{H}]$), and dust depletion (from $[\text{Cr}/\text{Zn}]$), we can use the measured values of $N(\text{Ca II})$ – determined via $W_0^{\lambda 3935}$ – to estimate the ratio $n(\text{Ca}^{2+})/n(\text{Ca}^+)$. For a range of values of the intensity of the far-UV radiation field (which determines the photoionisation rate Γ) we can then deduce the corresponding values of gas density $n(\text{H}_{\text{TOT}})$ (on which $n(e)$ depends), and thereby assess the hypothesis the gas volume density is the important factor regulating the strength of Ca II absorption. This, in turn, may shed light on the nature of the strong Ca II absorbers and their relationship, for example, to DLAs with associated molecular hydrogen absorption (Srianand et al. 2005).

4.3.1 Photoionisation models

With this aim, we ran series of photoionisation models with the software package CLOUDY⁴ (Ferland et al. 1998; Ferland 2000), approximating the DLAs as slabs of constant density gas irradiated by the metagalactic ionising background (Haardt & Madau 2001) and the cosmic microwave background at the appropriate redshift. We further added cosmic rays and an interstellar radiation field due to the OB stars within the galaxies giving rise to the DLAs; the spectral distribution of this last component was assumed to be the same as that of the interstellar radiation field in the solar vicinity, as given by Black (1987). For each DLA in Tables 1 and 2 where Zn II and Cr II lines were detected, we adopted the metallicity implied by the measures of $[\text{Zn}/\text{H}]$ (thereby assuming the dust depletion of Zn to be negligible in DLAs) and included dust grains with an abundance scaled with the DLA metallicity. We explicitly accounted for the depletion

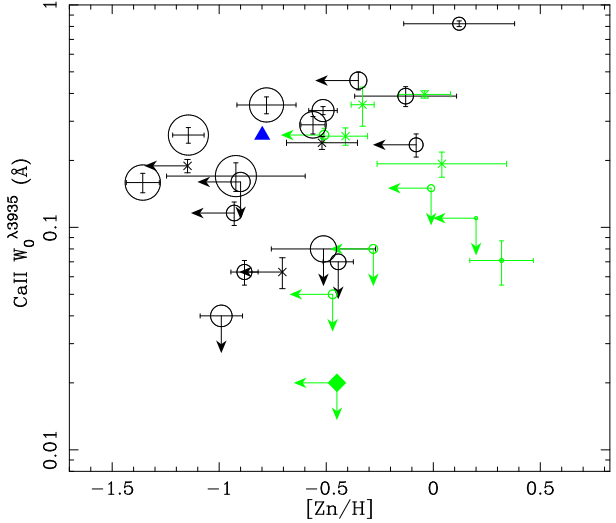


Figure 6. The rest-frame equivalent width of the Ca II $\lambda 3935$ line plotted as a function of DLA metallicity. The symbols have the same meaning as in Figure 5, except that the size of the open circles is now proportional to $N(\text{H I})$. SubDLAs are shown in green; for some of these, the assumption $N(\text{Zn II})/N(\text{H I}) = \text{Zn}/\text{H}$ adopted in section 3 may not be correct, possibly leading to an overestimate of the metallicity if some of the Zn II is associated with ionised gas.

of metals onto grains by assuming solar relative abundances as given by Lodders (2003), and a depletion pattern motivated by the well-studied interstellar cloud in front of the star ζ Oph (Savage & Sembach 1996). We scaled the level of depletion for each element more highly refractory than Zn based on our $[\text{Cr}/\text{Zn}]$ measurement:

$$[\text{X}/\text{Zn}]_{\text{gas}} = A(\text{X}) \times [\text{Cr}/\text{Zn}]_{\text{gas}}, \quad (2)$$

where $A(\text{X})$ is determined from the depletion values given by Savage & Sembach. This functional form matches the relative degrees of depletion from the gas-phase in the ISM towards ζ Oph, while reducing to $[\text{X}/\text{Zn}]_{\text{gas}} = 0$ when $[\text{Cr}/\text{Zn}]_{\text{gas}} = 0$ (i.e. when Cr is undepleted, so are all other metals).

Each model was characterised by a pair of values: gas density and intensity of the external stellar radiation field. We then used CLOUDY to predict the value of $N(\text{Ca II})$ appropriate to that model given the measured $N(\text{H I})$ and all of the above parameters. We assigned a χ^2 confidence level to each model, by comparing predicted and observed values of $N(\text{Ca II})$ and taking into account the uncertainties in our measurements of column densities. We assumed an uncertainty of ± 0.3 applied to the scaling factor in eq.(2) for Ca; i.e., $A(\text{Ca}) = 1.9 \pm 0.3$. Although *ad hoc*, it is likely a conservative estimate. The relative contribution to the total error arising from this uncertainty depends on the level of depletion, and ranged between zero and 50 per cent, with an average of 25 per cent, in our models. Thus, for each DLA in Tables 1 and 2 with measured $N(\text{Zn II})$ and $N(\text{Cr II})$ we were able to produce confidence intervals in gas density (cm^{-3}) for a given choice of intensity of the interstellar radiation field (in units of the local ISM radiation field intensity).

Figure 8 shows the 1σ ranges in gas density if the intensity of the interstellar radiation field is allowed to vary

⁴ <http://www.nublado.org/>

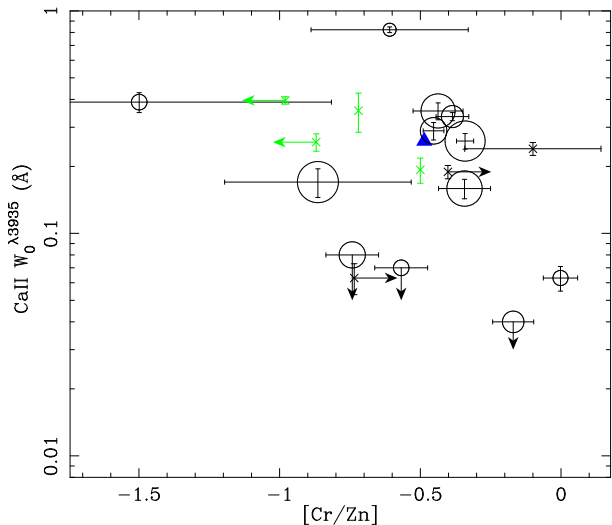


Figure 7. The rest-frame equivalent width of the Ca II $\lambda 3935$ line plotted as a function of Cr depletion. The symbols have the same meaning as in Figure 6.

between 1/10 and three times the reference value appropriate to our location within the Milky Way. We see that, even in the best cases, we only constrain $n(\text{H}_{\text{TOT}})$ to within ≈ 1 –2 orders of magnitude, depending on the level of star formation activity in the galaxies hosting the DLAs (since the star formation rate is presumably the main determinant of the radiation field intensity). Previous estimates of the interstellar radiation field intensity in DLAs have been deduced from consideration of the relative populations of the rotationally excited levels of the H_2 molecule (e.g. Ge & Bechtold 1997). Available data indicate a UV field intensity comparable to the local value (Srianand et al. 2005), consistent with the conclusion from most imaging studies that the galaxies giving rise to DLAs are generally fainter than L^* (Rao et al. 2003 and reference therein).

These measurements refer to DLAs at redshifts $z \gtrsim 2$ and it is thus unclear to what extent they also apply to lower redshift systems. If we assume, as a working assumption, a UV field equal to that observed locally, we obtain the values of gas density shown in Figure 9 and listed in Table 3 (where the DLAs are now listed in increasing order of $W_0^{\lambda 3935}$). The range of $W_0^{\lambda 3935}$ in our sample is too small, and in some cases $n(\text{H}_{\text{TOT}})$ is too poorly constrained, to discern an overall correlation between $W_0^{\lambda 3935}$ and $n(\text{H}_{\text{TOT}})$. However, we note that in the DLA with the lowest measured value of $W_0^{\lambda 3935}$ (at $z_{\text{abs}} = 0.8591$ in 0454+039, with $W_0^{\lambda 3935} = 0.063 \text{ \AA}$) we deduce the lowest value of gas density, $n(\text{H}_{\text{TOT}}) \simeq 0.1 \text{ cm}^{-3}$. Such a weak Ca II line cannot be ascribed to dust depletion of Ca, since in this DLA the Cr/Zn ratio is solar. Conversely, the only ‘strong’ Ca II absorber in our sample, according to the definition by WHP06 (at $z_{\text{abs}} = 0.7156$ in 1323–0021, with $W_0^{\lambda 3935} = 0.82 \text{ \AA}$), requires relatively high density according to our modelling, with $n(\text{H}_{\text{TOT}}) \simeq 7 \text{ cm}^{-3}$. In this, as in other DLAs with large values of $W_0^{\lambda 3935}$, we may have underestimated $N(\text{Ca II})$, and therefore $n(\text{H}_{\text{TOT}})$ (by ~ 0.1 – 0.5 dex), if there is hidden saturation in the absorption lines.

We can apply a similar analysis to the ‘low- $W_0^{\lambda 3935}$, ($\langle W_0^{\lambda 3935} \rangle = 0.49 \text{ \AA}$) and ‘high- $W_0^{\lambda 3935}$, ($\langle W_0^{\lambda 3935} \rangle = 1.01 \text{ \AA}$)

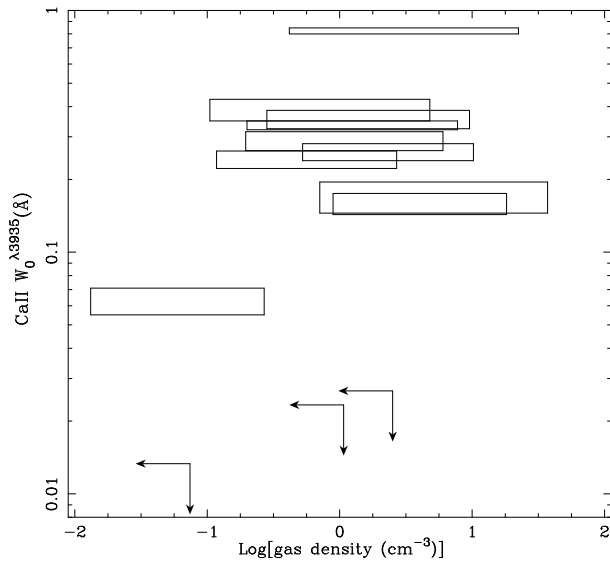


Figure 8. The rest-frame equivalent width of the Ca II $\lambda 3935$ line plotted as a function of the values of $n(\text{H}_{\text{TOT}})$ deduced from our CLOUDY modelling. The range of values of $n(\text{H}_{\text{TOT}})$ shown corresponds to the full range of normalisations of the UV radiation field considered in our modelling, from 1/10 to three times the local interstellar value. Upper-limits for $W_0^{\lambda 3935}$ and $n(\text{H}_{\text{TOT}})$ are shown at one-sigma.

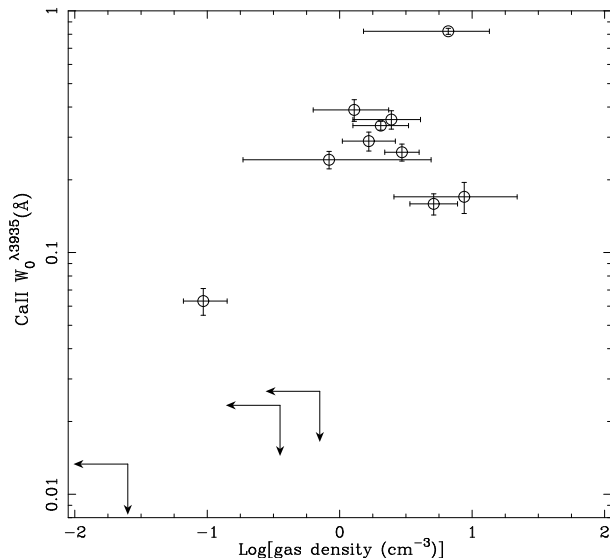


Figure 9. As for Figure 8, but now assuming that the interstellar radiation fields in the galaxies hosting the DLAs have the same intensity as that of the Milky Way near the Sun.

subsamples of Ca II absorbers from WHP06, for which those authors measured values of $N(\text{Ca II})$, $N(\text{Zn II})$, and $N(\text{Cr II})$ from composites of SDSS spectra. Since we do not know the value of $N(\text{H I})$ appropriate to these composites, we have performed the calculation for a range of values of the neutral hydrogen column density (and therefore also a range of metallicities). For typical DLA $N(\text{H I})$ -values, we find that, for a normalisation of the UV field equal to the local value, the typical strong Ca II absorber arises in gas with density in the range $n(\text{H}_{\text{TOT}}) \simeq 10^{0.8} - 10^{1.3} \text{ atoms cm}^{-3}$

for the low- $W_0^{\lambda 3935}$ subsample, and $n(\text{H}_{\text{TOT}}) \simeq 10^{1.1} - 10^{1.6}$ atoms cm^{-3} , for the high- $W_0^{\lambda 3935}$ subsample, depending on the value of $N(\text{H I})$.

4.3.2 Connection with H_2 ?

The current evidence thus suggests that strong Ca II absorbers trace gas of relatively high density. Returning to our sample, it can be seen from Figure 9 and Table 3 that if the UV radiation field intensity is comparable to that in the solar neighbourhood, most Ca II-bearing DLAs, and all four with $W_0^{\lambda 3935} \gtrsim 0.35 \text{ \AA}$, likely arise in gas with densities greater than ~ 1 atom cm^{-3} , while for the average Ca II system of WHP06 we find densities $\gtrsim 10$ atom cm^{-3} . These values approach the range derived by Srianand et al. (2005) in DLAs at $z > 2$ also exhibiting H_2 absorption, from consideration of the relative populations of the fine-structure levels of the ground state of C I. These authors propose that such systems trace the ‘Cold Neutral’ phase of the interstellar medium in galaxies; our study raises the possibility that absorption systems selected from their strong Ca II absorption may be the counterpart of such DLAs at lower redshift. In the last column of Table 3, we list the molecular fraction, $f_{\text{H}_2} = 2N(\text{H}_2)/(2N(\text{H}_2)+N(\text{H I}))$, predicted by our CLOUDY models for a normalization of the local UV field of unity. The range of values is broadly consistent with those found by Noterdaeme et al. (2008) for DLAs at redshifts $2 \lesssim z \lesssim 4$, although we predict a smaller fraction of very low f_{H_2} -values. However, the lowest f_{H_2} -values in the Noterdaeme et al. sample are dominated by the systems with the lowest metallicity and depletion, both of which are (on average) greater at the redshifts of our sample (Figures 3 and 4). If we consider only systems with metallicities greater than $\simeq -1.3$ in the high- z Noterdaeme et al. sample, the values predicted by CLOUDY are in reasonable agreement with observed molecular fractions. For DLAs with properties similar to the low- $W_0^{\lambda 3935}$ and high- $W_0^{\lambda 3935}$ subsamples of WHP06, our models predict $f_{\text{H}_2} \simeq -2.8$ to -2.1 and $f_{\text{H}_2} \simeq -0.4$, respectively. If these interpretations are correct, we expect that future space-based observations of strong Ca II absorbers at far-UV wavelengths will show not only a damped Ly α line, but also detectable levels of H_2 absorption.

At present, we can test this prediction with only three reported measurements of, or limits on, $N(\text{H}_2)$ at $z_{\text{abs}} < 1.3$: in the DLAs towards 0454+039 (which is in our sample) and 1328+307 ($z_{\text{abs}} = 0.692$; $N(\text{H I}) = 10^{21.28} \text{ cm}^{-2}$), and in the subDLA towards 0515-4414 ($z_{\text{abs}} = 1.1508$; $N(\text{H I}) = 10^{19.88} \text{ cm}^{-2}$ – see Table 2.) Molecular hydrogen is undetected in either of the two DLAs (Ge & Bechtold 1999), with $N(\text{H}_2) < 10^{16.38}$ and $f_{\text{H}_2} < 10^{-4.01}$ for the system towards 0454+039 and $N(\text{H}_2) < 10^{15.70}$ and $f_{\text{H}_2} < 10^{-5.28}$ for the system towards 1328+307. The former has the weakest detected Ca II line in our sample. For the latter, we estimate $W_0^{\lambda 3935} \lesssim 0.2 \text{ \AA}$ from its SDSS spectrum. Thus, neither of these two DLAs are strong Ca II absorbers. In contrast, the subDLA towards 0515-4414 does exhibit H_2 absorption (Reimers et al. 2003), with $N(\text{H}_2) = 10^{16.94 \pm 0.30}$ and $f_{\text{H}_2} = 10^{-2.64 \pm 0.30}$. In this system, $W_0^{\lambda 3935} = 0.36 \text{ \AA}$; while this does not qualify it as a ‘strong’ Ca II absorber in the sense defined by WHP06, we note that this value of $W_0^{\lambda 3935}$ is unusually high considering the low $N(\text{H I})$ (see

Table 3. PREDICTED GAS DENSITIES AND MOLECULAR FRACTIONS^a

| QSO | $W_0^{\lambda 3935}$ (\AA) | $\log n(\text{H}_{\text{TOT}})$ (cm^{-3}) | $\log f_{\text{H}_2}$ |
|------------------------|--|---|-----------------------|
| 0449–168 ^b | < 0.03 | < –1.6 | < –9.4 |
| 1733+5533 ^b | < 0.02 | < –0.45 | < –6.6 |
| 1007+0042 ^b | < 0.03 | < –0.14 | < –5.5 |
| 0454+039 | 0.06 ± 0.01 | $-1.03^{+0.18}_{-0.15}$ | –8.5 |
| 1727+5302 | 0.16 ± 0.02 | 0.71 ± 0.18 | –3.9 |
| 2353–0028 | 0.17 ± 0.03 | $0.94^{+0.41}_{-0.53}$ | –1.2 |
| 2328+0022 | 0.24 ± 0.02 | $-0.08^{+0.77}_{-0.65}$ | –6.3 |
| 1010+0003 | 0.26 ± 0.02 | 0.47 ± 0.13 | –3.6 |
| 1727+5302 | 0.29 ± 0.03 | 0.22 ± 0.20 | –3.1 |
| 1107+0048 | 0.34 ± 0.01 | 0.31 ± 0.21 | –3.1 |
| 1225+0035 | 0.36 ± 0.03 | $0.39^{+0.22}_{-0.29}$ | –2.6 |
| 0256+0110 ^c | 0.39 ± 0.04 | $0.11^{+0.26}_{-0.31}$ | –3.3 |
| 1323–0021 | 0.82 ± 0.02 | $0.82^{+0.31}_{-0.64}$ | –0.6 |

^aAssuming that the intensity of the stellar UV radiation field in the DLAs is similar to the mean value measured in the interstellar medium of the Milky Way near the Sun. Upper-limits correspond to one-sigma confidence bounds.

^b One-sigma upper-limits on $W_0^{\lambda 3935}$ were used in the models.

^cWe use the $\log N(\text{Cr II})$ value given in the literature for modelling the DLA towards 0256+0110 as our measurement is highly uncertain.

Figure 5). For comparison, in the lone strong Ca II system in our sample, $W_0^{\lambda 3935}$ is greater only by a factor of about two, despite having column densities of Zn II and Cr II one order of magnitude higher. It will be of interest to verify the extent to which $W_0^{\lambda 3935}$ and $N(\text{H}_2)$ are related as more measurements of these quantities become available.

5 SUMMARY AND CONCLUSIONS

We have used the WHT telescope on La Palma to record at intermediate resolution the optical spectra of QSOs known to lie behind DLAs and subDLAs in the redshift range $0.6 < z_{\text{abs}} < 1.3$. Our principal aims were twofold: (i) to measure the strength of the Ca II $\lambda\lambda 3935, 3970$ absorption lines in known DLAs, with a view to establishing to what extent DLAs and strong Ca II absorbers overlap; and (ii) to measure the Zn II $\lambda\lambda 2026, 2063$ and Cr II $\lambda\lambda 2056, 2062, 2066$ multiplets in the (sub)DLAs, thereby increasing the number of metallicity and depletion determinations in (sub)DLAs at low-redshift. By design, these complementary measurements allow us to test whether the strength of Ca II absorption is related to the metallicity of the gas, as measured by the abundance of Zn, and/or to the degree of dust depletion of refractory elements (both Ca and Cr are readily incorporated onto dust, whereas Zn is not). From consideration of such measurements in a sample of 16 DLAs and six subDLAs, augmented by similar data for three DLAs and four subDLAs from published studies, we reach the following conclusions.

1. The new measurements presented here strengthen previous conclusions on the metallicities and dust depletions in DLAs at $z < 1.3$. We point out that, after accounting for the fact that at these redshifts DLAs have mostly been selected from Mg II-strong systems – and may thus be bi-

ased in favour of metal-rich absorbers – the already weak redshift evolution of the mean DLA metallicity is reduced further: $[\langle \text{Zn}/\text{H} \rangle]$ is only a factor of about two greater at $0.6 < z < 1.3$ than at higher redshifts. We also confirm the dependence of dust depletion on metallicity uncovered by earlier studies.

2. Most DLAs exhibit detectable Ca II $\lambda 3935$ absorption in our spectra. Our new data indicate that selecting absorption systems above the threshold $W_0^{\lambda 3935} = 0.15 \text{ \AA}$ isolates systems with $N(\text{H I}) \gtrsim 2 \times 10^{20} \text{ cm}^{-2}$ (although with some contamination from subDLAs, as evidenced by detections reported in the literature). However, while it seems likely that strong Ca II absorption is associated with DLAs, the converse is not true: approximately one third of the DLAs in our sample have $W_0^{\lambda 3935} < 0.15 \text{ \AA}$, while adopting the criterion $W_0^{\lambda 3935} > 0.30 \text{ \AA}$ would miss $\simeq 3/4$ of the DLAs.

3. Only four out of the 19 DLAs in the combined sample meet the selection criterion $W_0^{\lambda 3935} \geq 0.35 \text{ \AA}$ of the SDSS survey by WHP6, and only one out of 19 would be classed as a ‘strong’ Ca II absorber by their definition ($W_0^{\lambda 3935} \geq 0.5 \text{ \AA}$). Evidently, there is little overlap as yet between confirmed DLAs and the SDSS candidates identified via Ca II. This is not surprising, however, since – as demonstrated by WHP06 – dust associated with many of the strong Ca II absorbers dims the light from the background QSOs sufficiently for them to be excluded from the magnitude-limited surveys conducted with *HST* up to now.

4. Overall, we find no convincing correlation of the strength of Ca II absorption with the column density of neutral gas, the equivalent width of Mg II $\lambda 2796$, the metallicity of the gas (as measured from the abundance of Zn), or the degree of depletion of refractory elements (indicated by the $[\text{Cr}/\text{Zn}]$ ratio). Despite the fact that, in the interstellar medium of the Milky Way, both Ca and Cr exhibit large and variable depletion factors from the gas-phase, DLAs with near-solar values of $[\text{Cr}/\text{Zn}]$ do not show significantly stronger Ca II lines than those where most of the Cr is presumably in solid form. On the other hand, the finding that the only ‘strong’ Ca II absorber in our sample is the most metal-rich DLA yet discovered suggests that there may be some connection between the metallicity and Ca II equivalent width.

5. Presumably, a more complex mix of factors than simply H I column density, metallicity, and dust depletion, determines the value of $W_0^{\lambda 3935}$ in DLAs. We have presented preliminary evidence that the ‘joker in the pack’ may be the variable fraction of Ca which is singly ionised in H I regions, where Ca III is often the dominant ion stage, depending on the densities of particles, far-UV photons, and on the temperature of the gas.

With the data at hand, we exploit the ionisation balance of Ca to place constraints on the ratio of UV photons and particles. If we further assume that the interstellar radiation field in the DLAs is of the same order as that at our location within the Milky Way – as indeed found for DLAs at higher redshifts – we can arrive at estimates of, or limits on, the gas density $n(\text{H}_{\text{TOT}})$. Our modelling, using the photoionisation code CLOUDY, indicates values $n(\text{H}_{\text{TOT}}) \gtrsim 1 \text{ cm}^{-3}$ for most DLAs with $W_0^{\lambda 3935} \gtrsim 0.35 \text{ \AA}$. Furthermore, for an ‘average’ Ca II-absorber DLA (as described by WHP06) as well as the lone ‘strong’ (as defined by those authors) Ca II system in our sample, we deduce $n(\text{H}_{\text{TOT}}) \gtrsim 10 \text{ cm}^{-3}$. Such high

values are similar to those which seem to be typical of H₂-bearing DLAs at $z > 2$, raising the possibility that in the strong Ca II absorbers selected by WHP06 at $z < 1.3$ we may be seeing the lower redshift counterparts of the subset of DLAs with a measurable molecular fraction. Indeed, our models predict molecular fractions similar to those reported for relatively metal-rich DLAs at high- z , with the strongest Ca II absorbers exhibiting values consistent with the highest reported measurements of f_{H_2} in DLAs.

If borne out by additional studies, the possible connection of strong Ca II absorbers to metal- and relatively molecule-rich gas has intriguing consequences when considered in light of the imaging results of Hewett & Wild (2007). It would mean that strong Ca II absorbers select gas with these properties not only in galactic disks, but also at distances of tens of kpc from relatively bright galaxies. Such a conclusion would be highly relevant to models of galactic outflows and star-formation feedback.

The currently observed population of DLAs are *not*, in general, strong Ca II absorbers. However, if most or all strong Ca II absorbers are DLAs and the true incidence of strong Ca II absorbers is as high as calculated by WHP06, these intriguing systems may represent a (potentially metal-rich) subset of DLA absorbers that are being missed from the current surveys. It will be possible to make progress towards clarifying this and other questions raised by the present work with COS measurements of metal lines and $N(\text{H I})$ in a sample of *known* strong Ca II absorbers. Like the rest of the UV-spectroscopy community, we look forward with anticipation to the forthcoming *HST* servicing mission that will install this much needed instrument.

ACKNOWLEDGMENTS

The authors wish to thank Bob Carswell (VPFIT), and Gary Ferland and Ryan Porter (CLOUDY) for providing, maintaining, and offering help with their software. We are grateful to the WHT time assignment committee for their support of this programme and to the staff astronomers on La Palma for their help with the observations. DBN, MP and PCH acknowledge support from the STFC-funded Galaxy Formation and Evolution programme at the Institute of Astronomy. VW is supported by the MAGPOP Marie Curie EU Research and Training Network.

REFERENCES

- Akerman, C. J., Ellison, S. L., Pettini, M., & Steidel, C. C. 2005, *A&A*, 440, 499
- Black, J. H. 1987, in *Interstellar Processes*, (Dordrecht, D. Reidel Publishing Co.) 731
- Cayrel, R., et al. 2004, *A&A*, 416, 1117
- de la Varga, A., Reimers, D., Tytler, D., Barlow, T., & Burles, S. 2000, *A&A*, 363, 69
- Ellison, S. L., Yan, L., Hook, I. M., Pettini, M., Wall, J. V., & Shaver, P. 2001, *A&A*, 379, 393
- Ferland, G. J. 2000, in *Revista Mexicana de Astronomia y Astrofisica Conference Series*, ed. S. J. Arthur, N. S. Brickhouse, & J. Franco, 153
- Ferland, G. J., Korista, K. T., Verner, D. A., Ferguson, J. W., Kingdon, J. B., & Verner, E. M. 1998, *PASP*, 110, 761

- Fox, A. J., Petitjean, P., Ledoux, C., & Srianand, R. 2007a, *A&A*, 465, 171
- Fox, A. J., Petitjean, P., Ledoux, C., & Srianand, R. 2007b, *ApJL*, 668, L15
- Ge, J., & Bechtold, J. 1997, *ApJL*, 477, L73
- Ge, J., & Bechtold, J. 1999, in Carilli, C. L., Radford, S. J. E., Menten, K. M., Langston, G. I., eds, *Highly Redshifted Radio Lines*, *Astron. Soc. Pac.*, San Francisco, p. 738
- Haardt F., & Madau P. 2001, in *Clusters of Galaxies and the High Redshift Universe Observed in X-rays* Neumann, D. M. and Tran, J. T. V., eds.
- Hewett, P. C., & Wild, V. 2007, *MNRAS*, 379, 738
- Jenkins, E. B., & Tripp, T. M. 2006, *ApJ*, 637, 548
- Jorgenson, R. A., Wolfe, A. M., Prochaska, J. X., Lu, L., Howk, J. C., Cooke, J., Gawiser, E., & Gelino, D. M. 2006, *ApJ*, 646, 730
- Kennicutt, R. C., Jr. 1998, *ApJ*, 498, 541
- Khare P., Kulkarni V. P., Lauroesch J. T., York D. G., Crotts A. P. S., Nakamura O., 2004, *ApJ*, 616, 86
- Kulkarni, V. P., Fall, S. M., Lauroesch, J. T., York, D. G., Welty, D. E., Khare, P., & Truran, J. W. 2005, *ApJ*, 618, 68
- Kulkarni, V. P., Khare, P., Péroux, C., York, D. G., Lauroesch, J. T., & Meiring, J. D. 2007, *ApJ*, 661, 88
- Lah, P., et al. 2007, *MNRAS*, 376, 1357
- Ledoux C., Petitjean P., Srianand R., 2003, *MNRAS*, 346, 209
- Lodders, K. 2003, *ApJ*, 591, 1220
- Marschall, L. A., & Hobbs, L. M. 1972, *ApJ*, 173, 43
- Massey, P., Strobel, K., Barnes, J. V., & Anderson, E. 1988, *ApJ*, 328, 315
- Meiring, J. D., et al. 2006, *MNRAS*, 370, 43
- Meiring, J. D., Lauroesch, J. T., Kulkarni, V. P., Péroux, C., Khare, P., York, D. G., & Crotts, A. P. S. 2007, *MNRAS*, 376, 557
- Meiring J. D., Kulkarni V. P., Lauroesch J. T., Péroux C., Khare P., York D. G., Crotts A. P. S., 2008, *MNRAS*, 384, 1015
- Meyer, D. M., Welty, D. E., & York, D. G. 1989, *ApJL*, 343, L37
- Morton, D. C. 2003, *ApJS*, 149, 205
- Morton, D. C., Drake, J. F., Jenkins, E. B., Rogerson, J. B., Spitzer, L., & York, D. G. 1973, *ApJL*, 181, L103
- Murphy, M. T., Curran, S. J., Webb, J. K., Ménager, H., & Zych, B. J. 2007, *MNRAS*, 376, 673
- Nestor, D. B., Rao, S. M., Turnshek, D. A., & Vanden Berk, D. 2003, *ApJL*, 595, L5
- Nestor, D. B., Turnshek, D. A., & Rao, S. M. 2005, *ApJ*, 628, 637
- Nissen, P. E., Akerman, C., Asplund, M., Fabbian, D., Kerber, F., Kaufl, H. U., & Pettini, M. 2007, *A&A*, 469, 319
- Noterdaeme P., Ledoux C., Petitjean P., Srianand R., 2008, *A&A*, 481, 327
- Péroux, C., Meiring, J. D., Kulkarni, V. P., Ferlet, R., Khare, P., Lauroesch, J. T., Vladilo, G., & York, D. G. 2006a, *MNRAS*, 372, 369
- Péroux C., Kulkarni V. P., Meiring J., Ferlet R., Khare P., Lauroesch J. T., Vladilo G., York D. G., 2006b, *A&A*, 450, 53
- Péroux C., Meiring J. D., Kulkarni V. P., Khare P., Lauroesch J. T., Vladilo G., York D. G., 2008, *MNRAS*, 493
- Pettini, M. 2006 in *The Fabulous Destiny of Galaxies: Bridging Past and Present*, V. LeBrun, A. Mazure, S. Arnouts & D. Burgarella eds., (Paris: Frontier Group), 319 (astro-ph/0603066).
- Pettini, M., Boksenberg, A., & Hunstead, R. W. 1990, *ApJ*, 348, 48
- Pettini, M., Smith, L. J., Hunstead, R. W., & King, D. L. 1994, *ApJ*, 426, 79
- Pettini, M., King, D. L., Smith, L. J., & Hunstead, R. W. 1997a, *ApJ*, 478, 536
- Pettini, M., Smith, L. J., King, D. L., & Hunstead, R. W. 1997b, *ApJ*, 486, 665
- Prochaska, J. X., Herbert-Fort, S., & Wolfe, A. M. 2005, *ApJ*, 635, 123
- Prochaska, J. X., Wolfe, A. M., Howk, J. C., Gawiser, E., Burles, S. M., & Cooke, J. 2007, *ApJS*, 171, 29
- Quast, R., Reimers, D., & Baade, R. 2008, *A&A*, 477, 443
- Rao S. M., Nestor D. B., Turnshek D. A., Lane W. M., Monier E. M., Bergeron J., 2003, *ApJ*, 595, 94
- Rao S. M., 2005, in Williams, P. R., Shu, C.-G., Menard, B. eds, *Probing Galaxies through Quasar Absorption Lines*, Cambridge Univ. Press, p. 125
- Rao, S. M., Turnshek, D. A., & Nestor, D. B. 2006, *ApJ*, 636, 610 (RTN06)
- Reimers, D., Baade, R., Quast, R., & Levshakov, S. A. 2003, *A&A*, 410, 785
- Rix, S. A., Pettini, M., Steidel, C. C., Reddy, N. A., Adelberger, K. L., Erb, D. K., & Shapley, A. E. 2007, *ApJ*, 670, 15
- Savage, B. D., & Sembach, K. R. 1996, *ARA&A*, 34, 279
- Srianand, R., Petitjean, P., Ledoux, C., Ferland, G., & Shaw, G. 2005, *MNRAS*, 362, 549
- Viegas, S. M. 1995, *MNRAS*, 276, 268
- Vladilo, G. 2002, *ApJ*, 569, 295
- Vladilo, G., Centurión, M., Bonifacio, P., & Howk, J. C. 2001, *ApJ*, 557, 1007
- Vladilo, G., Prochaska, J. X., & Wolfe, A. M. 2008, *A&A*, in press
- Welty, D. E., Morton, D. C., & Hobbs, L. M. 1996, *ApJS*, 106, 533
- Wild V., Hewett P. C., 2005, *MNRAS*, 361, L30
- Wild, V., Hewett, P. C., & Pettini, M. 2006, *MNRAS*, 367, 211 (WHP06)
- Wild V., Hewett P. C., Pettini M., 2007, *MNRAS*, 374, 292
- Wolfe A. M., Turnshek D. A., Smith H. E., Cohen R. D., 1986, *ApJS*, 61, 249
- Wolfe, A. M., & Chen, H.-W. 2006, *ApJ*, 652, 981
- Wolfe A. M., Gawiser E., Prochaska J. X., 2005, *ARA&A*, 43, 861
- Zych, B. J., Murphy, M. T., Pettini, M., Hewett, P. C., Ryan-Weber, E. V., & Ellison, S. L. 2007, *MNRAS*, 379, 1409

**APPENDIX A: QSO COORDINATES,
MAGNITUDES, AND REDDENING
ESTIMATES**

Here we list the celestial coordinates, magnitudes, and estimates of $E(B - V)$ for the quasars listed in Tables 1 and 2. Magnitudes are given for the SDSS i' filter, when possible. $E(B - V)$ for systems in our sample with an available SDSS spectrum is estimated exactly as in Wild & Hewett (2005). Note that the scatter in individual reddening values (due to the intrinsic variation in the quasar SEDs from object to object) cause some ‘negative reddenings’ to occur.

| Name | Ra (J2000) | Dec (J2000) | $m_{i(AB)}$ | $E(B - V)$ |
|-----------|-------------|-------------|--------------|------------|
| 0139-0023 | 01 39 38.71 | -00 23 48.1 | 18.57 | -0.099 |
| 0253+0107 | 02 53 16.46 | +01 07 59.8 | 18.56 | +0.001 |
| 0256+0110 | 02 56 07.24 | +01 10 38.7 | 18.42 | -0.031 |
| 0449-168 | 04 52 14.23 | -16 40 16.8 | $m_V = 17.0$ | ... |
| 0454+039 | 04 56 47.2 | +04 00 53 | $m_V = 16.5$ | ... |
| 1007+0042 | 10 07 15.54 | +00 42 58.4 | 18.75 | +0.029 |
| 1009-0026 | 10 09 30.47 | -00 26 19.2 | 17.28 | -0.118 |
| 1010+0003 | 10 10 18.20 | +00 03 51.2 | 18.03 | -0.039 |
| 1107+0048 | 11 07 29.04 | +00 48 11.2 | 17.19 | -0.036 |
| 1107+0003 | 11 07 36.68 | +00 03 29.6 | 18.04 | +0.089 |
| 1220-0040 | 12 20 37.01 | -00 40 32.4 | 18.33 | -0.022 |
| 1224+0037 | 12 24 14.30 | +00 37 09.0 | 18.53 | -0.052 |
| 1225+0035 | 12 25 56.62 | +00 35 35.0 | 18.52 | +0.072 |
| 1323-0021 | 13 23 23.79 | -00 21 55.3 | 17.64 | +0.220 |
| 1727+5302 | 17 27 39.03 | +53 02 29.2 | 18.04 | -0.028 |
| 1733+5533 | 17 33 22.99 | +55 33 00.9 | 17.86 | -0.018 |
| 2149+212 | 21 51 45.9 | +21 30 14 | $m_V = 19.0$ | ... |
| 2353-0028 | 23 53 21.63 | -00 28 40.7 | 18.23 | +0.025 |
| 0515-4414 | 05 17 07.61 | -44 10 56.2 | $m_B = 15.0$ | ... |
| 0738+313 | 07 41 10.70 | +31 12 00.2 | 16.66 | ... |
| 1436-0051 | 14 36 45.06 | -00 51 50.5 | 18.25 | ... |
| 2328+0022 | 23 28 20.37 | +00 22 38.2 | 17.78 | ... |
| 2331+0038 | 23 31 21.82 | +00 38 07.4 | 17.51 | ... |
| 2335+1501 | 23 35 44.19 | +15 01 18.4 | 18.22 | ... |